RESEARCH ARTICLE

A New Way of Sensing: Need-Based Activation of Antibiotic Resistance by a Flux-Sensing Mechanism

Georg Fritz,[a,b]* Sebastian Dintner,[a] Nicole Simone Treichel,[a] Jara Radeck,[a] Ulrich Gerland,[b]* Thorsten Mascher,[a]* Susanne Gebhard[a]*

Department Biology I, Ludwig-Maximilians-Universität München, Planegg-Martinsried, Germany[a]; Arnold Sommerfeld Center for Theoretical Physics, Ludwig-Maximilians-Universität München, Munich, Germany[b]

* Present address: Georg Fritz, LOEWE-Center for Synthetic Microbiology, Philipps-Universität Marburg, Marburg, Germany; Ulrich Gerland, Technische Universität München, Garching, Germany; Thorsten Mascher, Technische Universität Dresden, Institute of Microbiology, Dresden, Germany; Susanne Gebhard, Department of Biology and Biochemistry, University of Bath, Claverton Down, United Kingdom.

ABSTRACT **Sensing of and responding to environmental changes are of vital importance for microbial cells. Consequently, bacteria have evolved a plethora of signaling systems that usually sense biochemical cues either via direct ligand binding acting as "concentration sensors" or by responding to downstream effects on bacterial physiology, such as structural damage to the cell. Here, we describe a novel, alternative signaling mechanism that effectively implements a "flux sensor" to regulate antibiotic resistance. It relies on a sensory complex consisting of a histidine kinase and an ABC transporter, in which the transporter fulfills the dual role of both the sensor of the antibiotic and the mediator of resistance against it. Combining systems biological modeling with *in vivo* experimentation, we show that these systems in fact respond to changes in activity of individual resistance transporters rather than to changes in the antibiotic concentration. Our model shows that the cell thereby adjusts the rate of *de novo* transporter synthesis to precisely the level needed for protection. Such a flux-sensing mechanism may serve as a cost-efficient produce-to-demand strategy, controlling a widely conserved class of antibiotic resistance systems.**

IMPORTANCE **Bacteria have to be able to accurately perceive their environment to allow adaptation to changing conditions. This is usually accomplished by sensing the concentrations of beneficial or harmful substances or by measuring the effect of the prevailing conditions on the cell. Here we show the existence of a new way of sensing the environment, where the bacteria monitor the activity of an antibiotic resistance transporter. Such a "flux-sensing" mechanism allows the cell to detect its current capacity to deal with the antibiotic challenge and thus precisely respond to the need for more transporters. We propose that this is a cost-efficient way of regulating antibiotic resistance on demand.**

Received 11 June 2015 **Accepted** 22 June 2015 **Published** 21 July 2015

Citation Fritz G, Dintner S, Treichel NS, Radeck J, Gerland U, Mascher T, Gebhard S. 2015. A new way of sensing: need-based activation of antibiotic resistance by a flux-sensing mechanism. mBio 6(4):e00975-15. doi:10.1128/mBio.00975-15.

Editor George L. Drusano, University of Florida

Address correspondence to Thorsten Mascher, thorsten.mascher@tu-dresden.de.

Sensing of and responding to environmental changes are of vital importance for microbial cells, as they facilitate their fine-tuned adaptation to prevailing conditions. The range of parameters a single cell can monitor is immense, including conditions as diverse as nutrient supply, oxygen levels, temperature, pH, cell densities, and presence of toxic compounds. It is therefore hardly surprising that bacteria have developed a plethora of sensory and regulatory strategies to accomplish this feat. In the specific context of antibiotic resistance, bacteria have to be able to accurately determine the severity of the attack in order to decide on an adequate response. The precision of this response is key to both survival of antimicrobial action and minimizing the metabolic cost of resistance (1, 2).

One common feature of controlling a cellular response is to monitor the ambient concentration of a specific substance. In the case of antibiotic resistance, this can be achieved, e.g., via direct binding to a sensory protein, such as the vancomycin-responsive histidine kinase (HK) VanSsc of *Streptomyces coelicolor* (3). An alternative approach is to monitor the cellular damage caused by the antibiotic, as is the case, e.g., for the LiaRS cell envelope damage-sensing system of *Bacillus subtilis* (4). Such an indirect sensing strategy allows the cell to integrate its current physiological state, which can significantly influence the potency of a given concentration of antibiotic. For instance, fast-growing cells are usually much more susceptible to antibiotic action than slow-growing cells. While a damage-sensing strategy undoubtedly provides a more context-dependent response, it requires the accumulation of a certain degree of cellular damage. Here, we present evidence for a third, previously undescribed regulatory strategy, allowing the bacterium to directly monitor its current capacity to deal with the antibiotic threat by measuring the activity of a drug efflux pump (referred to as "flux sensing").

We recently showed that a unique type of ATP-binding cassette (ABC) transporters is actively involved in a signaling pathway controlling its own production (5–7). These transporters mediate resistance against a wide range of antimicrobial peptides in many Gram-positive species, including important pathogens, such as *Staphylococcus aureus* and *Enterococcus faecalis* (8). Their expres-

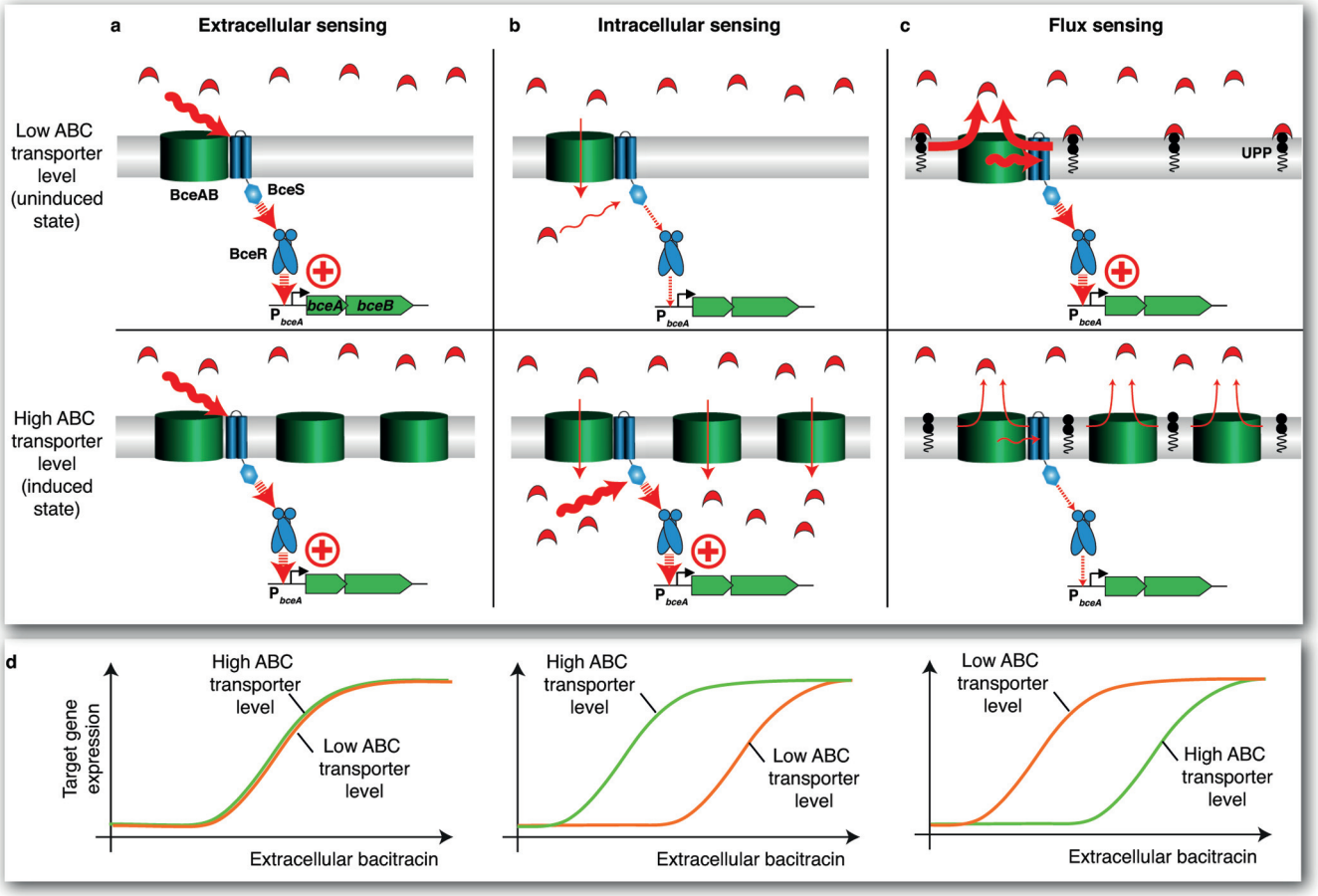

FIG 1 Schematic of conceivable sensory scenarios employed by the BceRS-BceAB system. In an external sensing scenario (a), the ABC transporter BceAB might act as a scaffold that keeps the histidine kinase BceS in an active conformation, which would allow BceS to perceive the extracellular concentration of bacitracin (red symbols). Since up-regulation of BceAB is not expected to change the extracellular concentration of bacitracin, the rate of gene expression should be independent of the BceAB level in this scenario (no feedback). In an internal sensing scenario (b), BceAB might be required to translocate bacitracin into the cytoplasm where BceS could sense its abundance. Here, up-regulation of BceAB should lead to an increased rate of bacitracin influx, which would in turn lead to further up-regulation of BceAB expression (positive feedback). In a flux-sensing scenario (c), BceAB itself is the true sensor, which directly signals its transport activity to BceS. In such a scenario, up-regulation of BceAB would reduce the load experienced by each individual transporter and thereby reduce signaling via BceS (negative feedback). (d) Schematic depiction of the expected impact of different levels of the BceAB transporter (low, red curves; high, green curves) on dose-dependent P_{bceA} activity.

sion is regulated by two-component systems whose HKs lack discernible ligand-binding domains and instead form a sensory complex with the transporter (9, 10). The signaling process is best understood in *Bacillus subtilis*, where the two-component system BceRS and its associated ABC-transporter BceAB together sense and counteract the deleterious effects of bacitracin and several other antimicrobial peptides interfering with the lipid II cycle of cell wall biosynthesis, by triggering a 500-fold increase in the expression of the *bceAB* transporter operon (5, 9, 11) (Fig. 1a).

To characterize the regulatory role of the transporter, here we took a systems approach, combining mathematical modeling with experiments probing the time-resolved, dose-dependent response of the Bce system to its substrate bacitracin. We show that signaling within the Bce system operates by a flux-sensing mechanism, monitoring the activity of individual transporters. Our model allowed us to derive a unique response signature for a flux sensor, which was experimentally validated. Moreover, the model was able to predict the antibiotic sensitivity of cells depending on transporter expression, leading us to propose that flux sensing serves as a novel produce-to-demand strategy to control antibiotic resistance in changing environments.

RESULTS

ABC transporter production rapidly adapts to a wide range of bacitracin inputs. To obtain detailed quantitative information on the regulatory dynamics of the Bce system, we first studied the relationship between the external antibiotic concentration and the transcriptional response of the target promoter P_{bceA}. To this end, exponentially growing SGB073 cells (wild-type *B. subtilis* carrying a chromosomally integrated P_{bceA}-*luxABCDE* reporter) were exposed to sublethal concentrations of bacitracin. At virtually all bacitracin concentrations tested, luciferase activity initially rose rapidly upon antibiotic addition, before leveling off to reach a plateau 20 to 30 min after induction (Fig. 2A). A plot of the plateau level against antibiotic concentration revealed that the system's response quickly adapted to a wide dynamic range of antibiotic

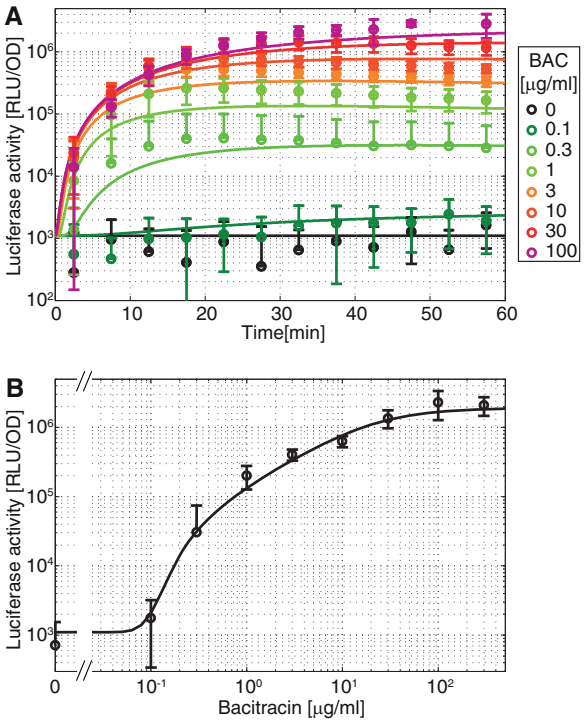

FIG 2 Gene expression driven by the P_{bceA} promoter rapidly adapts to a wide range of antibiotic concentrations. (A) Exponentially growing cells of strain SGB073 were exposed to sublethal concentrations of bacitracin at 0 min, and luciferase activity from a P_{bceA}-*luxABCDE* reporter construct was monitored over time. Data are means and standard deviations for at least three independent biological replicates (lower error bars are not depicted if negative values were reached). Lines show the dynamics predicted by the quantitative mathematical model described in the main text. (B) Experimental dose-response curve of the P_{bceA} promoter at a fixed time (42.5 min) after induction (symbols) and the fit to the mathematical model (lines). For details, see the text.

input (0.1 to 100 μg/ml bacitracin) (Fig. 2B). Such gradual, homeostatic control of target gene expression is often found in regulatory systems that exploit negative-feedback mechanisms, while positive-feedback regulation frequently enables switch-like or even hysteretic responses (12). The presence of a negative feedback mechanism was also suggested by our observation that the P_{bceA} promoter activity reached its steady-state value within a short time (20 to 30 min) (Fig. 2A) relative to the cell doubling time of ~70 min (see Fig. S1 in the supplemental material), as negative-feedback control is known to reduce the response time of genetic circuits (13).

To elucidate the source of this apparent feedback effect, we considered three plausible roles of the transporter in the regulatory pathway. (i) In the simplest scenario, the transporter acts as a mere ligand-binding component in a sensory complex with the HK, as is the case in regulation of sugar phosphate uptake by the Uhp system in *Escherichia coli* (14, 15). The input signal for such a system is the ambient concentration of the cognate substrate (Fig. 1a). This signal will not change if the number of transporters inserted in the membrane increases, since the amount of HK, and hence the number of sensory complexes, remains constant. Thus, there will be no feedback on regulation. (ii) Alternatively, the transporter might be required to translocate the substrate to a cytoplasmic recognition site (Fig. 1b). Such a strategy is realized, e.g., in the regulation of arabinose utilization by *E. coli* (16), where the level of intracellular substrate serves as the input signal. While the polarity of BceAB-mediated transport is not known, it has been suggested that BceAB may act as an importer of bacitracin, releasing it into the cytoplasm for degradation (5, 8). Here, the strength of the stimulus should increase during the induction process, because the amount of bacitracin transported into the cell will rise with the supply of transporters, thus creating a positive feedback on the response. (iii) The third conceivable scenario is that the HK activity is determined by the rate of flux through individual transporters (Fig. 1c). BceAB has also been proposed to act as a "hydrophobic vacuum cleaner" (17), conferring resistance by clearing the target from the inhibitory grip of the antibiotic (Fig. 1c) (7, 18). In such a scenario, increasing BceAB copy numbers should alleviate the load experienced by individual transporters (Fig. 1c), resulting in a negative feedback of BceAB on its own expression. Thus, qualitatively, a flux-sensing scenario best reflects the observed dynamics of P_{bceA} activation.

The behavior of the wild-type system is compatible with a mathematical model for relative flux sensing. To test if the proposed flux-sensing mechanism can quantitatively explain the regulatory dynamics in the Bce system, we developed a mathematical model, incorporating signal transduction via such a mechanism. Bacitracin is known to bind to its membrane-associated target molecule undecaprenol-pyrophosphate (UPP), thus blocking the dephosphorylation and recycling of UPP in the lipid II cycle of cell wall biosynthesis (19). If we suppose that the ABC transporter BceAB catalyzes the release of bacitracin from UPP with Michaelis-Menten enzyme kinetics, the time-dependent concentration of the bacitracin-bound form of UPP, UPP-bac, can be described by a differential equation of the form

$$\frac{d}{dt}[\text{UPP-bac}] = k^{\text{on}}[\text{bac}](\text{UPP}_{\text{tot}} - [\text{UPP-bac}]) - k^{\text{off}}[\text{UPP-bac}] - v_{\max}J_{\text{bac}}[\text{BceAB}] \quad (1)$$

Here, [bac] is the externally applied bacitracin concentration, k^{on} and k^{off} are the spontaneous on and off rates for the binding of bacitracin to UPP, UPP_{tot} is the total UPP level in the cell, $J_{\text{bac}} = [\text{UPP-bac}]/(K_m + [\text{UPP-bac}])$ is the relative bacitracin load per BceAB transporter, and $v_{\max}$ and K_m are the maximal transport rate and Michaelis-Menten constant of BceAB, respectively (see Tables S1 and S2 in the supplemental material).

To implement the proposed flux-sensing mechanism in our model, we took into account that the expression of the two-component system operon *bceRS* is constitutive (see Fig. S2 in the supplemental material) and also that the interaction between the histidine kinase BceS and the BceAB transporter is bacitracin independent (9). Moreover, we verified that the overproduction of BceS did not significantly affect the MIC of a strain with constitutive BceAB expression (see Fig. S3 in the supplemental material), indicating that the transport activity of BceAB is not affected by the formation of the sensory complex with BceS *in vivo*. Thus, as long as BceAB molecules outnumber BceS molecules, so that BceS is the limiting component in complex formation, there should be a constant number of functional BceS-BceAB sensory complexes in the cell, while the number of free BceAB transporters should change with increasing total transporter levels. Under inducing conditions this is a safe assumption, because we can readily detect the presence of BceAB, but not of BceS, using Western blotting or

fluorescent protein fusions (our unpublished observations). Under noninducing conditions, both proteins are below our current detection limit and therefore not accessible to quantification. Based on the relative promoter strengths of P_{bceR} (see Fig. S2 in the supplemental material) and P_{bceA} (Fig. 2A), it could well be that uninduced cells possess more kinases than transporters. Nevertheless, within our mathematical model we assume that the number of sensory complexes does not change over time and thus that BceS always monitors the activity of a fixed number of transporters. While this assumption might be inaccurate in the early phase of induction, BceAB levels are expected to quickly exceed those of BceS such that the model should well reflect the experimental conditions shortly after induction.

Based on these considerations, we assume within our model that BceS signals the load of individual transporters to the response regulator BceR, such that the level of the active (phosphorylated) form of BceR is proportional to the bacitracin load per transporter, J_{bac}. Following a thermodynamic model for transcriptional regulation (20), activation of gene expression from the P_{bceA} promoter by phosphorylated BceR can then be formulated in terms of J_{bac}, such that the dynamic equations for *bceAB* mRNA concentration, $[m]$, and BceAB protein level, [BceAB], read

$$\frac{d}{dt}[m] = \alpha\frac{1 + \omega(J_{\mathrm{bac}}/\kappa)^n}{1 + (J_{\mathrm{bac}}/\kappa)^n} - \lambda[m] \quad (2)$$

$$\frac{d}{dt}[\mathrm{BceAB}] = \beta[m] - \delta[\mathrm{BceAB}] \quad (3)$$

Here, α is the basal transcription rate, ω is the ratio of maximal to basal promoter activity, λ is the mRNA degradation rate, and κ is a measure of the relative flux at which P_{bceA} is activated. The Hill exponent (n) in turn reflects all forms of cooperativity in stimulus perception and signal transduction, as well as in BceR-DNA binding and recruitment of RNA polymerase. Finally, β is the translation rate and δ is the protein dilution rate due to cell doubling. The dynamic equations for luciferase reporter expression were formulated analogously to equations 2 and 3 and are given in Materials and Methods.

We then asked whether the data in Fig. 2 were in quantitative agreement with our mathematical model. To this end, all known and measured model parameters were fixed to their physiological values (see Table S1 in the supplemental material), the remaining ones were confined to physiological intervals (see Table S2 in the supplemental material), and then the model was fitted to the experimental dose-response in Fig. 2B (see Materials and Methods for details of the fitting procedure). Overall, we found that the dynamic behavior of the model closely resembled the rapid adaptation kinetics observed in the experimental time series (Fig. 2A). Likewise, the model adequately captured the gradual increase of the experimental dose-response characteristics over a wide range of input levels (Fig. 2B). These findings provided the first quantitative indication that the Bce system does in fact implement a flux-sensing mechanism that monitors the bacitracin load per BceAB transporter. The agreement between theory and experiment in the early phase (0 to 15 min) after induction further demonstrates that the model assumption of a constant number of sensory complexes per cell was reasonable: if BceAB were initially less abundant than BceS, the number of sensory complexes should increase upon induction of BceAB production, which should result in a positive feedback on signaling. Such a positive feedback should cause a lag in the response while the number of sensory complexes is still very low, followed by a rapid increase in signaling as more and more complexes are formed. Such an effect is not visible in our data (Fig. 2A), showing that the window in which the number of sensory complexes is not constant is short and cannot be resolved by the luciferase reporter.

Predicting the signature of a relative flux sensor. One key feature of the proposed flux sensor model is that up-regulation of BceAB leads to a reduction of the bacitracin load per transporter, which ultimately down-regulates transcription of *bceAB*. Hence, if the model was correct, disabling this negative autoregulation of BceAB should abolish the graded response to bacitracin. Consequently, constitutively supplying the cell with a fixed number of transporter molecules should provide an alternative means of distinguishing between the three different signaling scenarios detailed above. For a relative flux-sensing mechanism, in cells with few transporters, the load per transporter should be saturated at low bacitracin concentrations, leading to a highly sensitive response (Fig. 1d, right). Conversely, cells with many transporters should respond more sluggishly (Fig. 1d, right), because more bacitracin is required to produce a high load per transporter. For an intracellular sensing mechanism, the opposite behavior is expected: cells with a high level of BceAB should respond more sensitively than those with few transporters, as the total amount of bacitracin translocated increases with the number of transporters present (Fig. 1d, center). Last, for an extracellular-concentration-sensing mechanism, the dose-response behavior should not be affected by alterations in the level of the transporter (Fig. 1d, left). In fact, this last situation was recently reported for the DctA/DcuS sensor complex of *E. coli* (21), in which the transporter DctA merely acts as an activity switch for the HK DcuS.

When we modified our mathematical model to accommodate constitutive production of the transporter, the predicted dose-response behavior was altered in two respects. First, the elimination of autoregulation of the level of BceAB results in a more switch-like response of the P_{bceA} promoter to increasing bacitracin concentrations (Fig. 3a). This sharp response is due to the fact that the fit to the data for the wild type in Fig. 2 yielded a Hill exponent (n) of 7.5 ± 0.2, suggesting that signal transduction and regulation of P_{bceA} exhibit a high degree of cooperativity. Second, when the copy number of the transporter is changed, the model predicts a shift in the dose-response curves consistent with the signature of a flux sensor: in cells that constitutively express low levels of BceAB, the promoter is triggered by low bacitracin concentrations (Fig. 3a), while much higher concentrations of the antibiotic are required to activate P_{bceA} in cells that synthesize large amounts of BceAB (Fig. 3a).

In order to test these predictions experimentally, we constructed a strain (SGB218) in which the endogenous *bceAB* locus had been deleted, and replaced by a chromosomally integrated construct driven by the xylose-inducible promoter P_{xylA}. In addition, this strain carries the P_{bceA}-*luxABCDE* reporter used above. We previously quantified the dose-response characteristics of P_{xylA} (22). It showed a basal transcription level ~30-fold higher than that driven by P_{bceA} and could be activated up to ~100-fold by increasing the xylose concentration in the medium (Fig. 3b). Based on these data, we selected five xylose concentrations (0%, 0.005%, 0.01%, 0.03%, and 0.2%) that resulted in markedly different P_{xylA} activities. Incorporation of these promoter activities into our mathematical model led to distinct BceAB protein levels

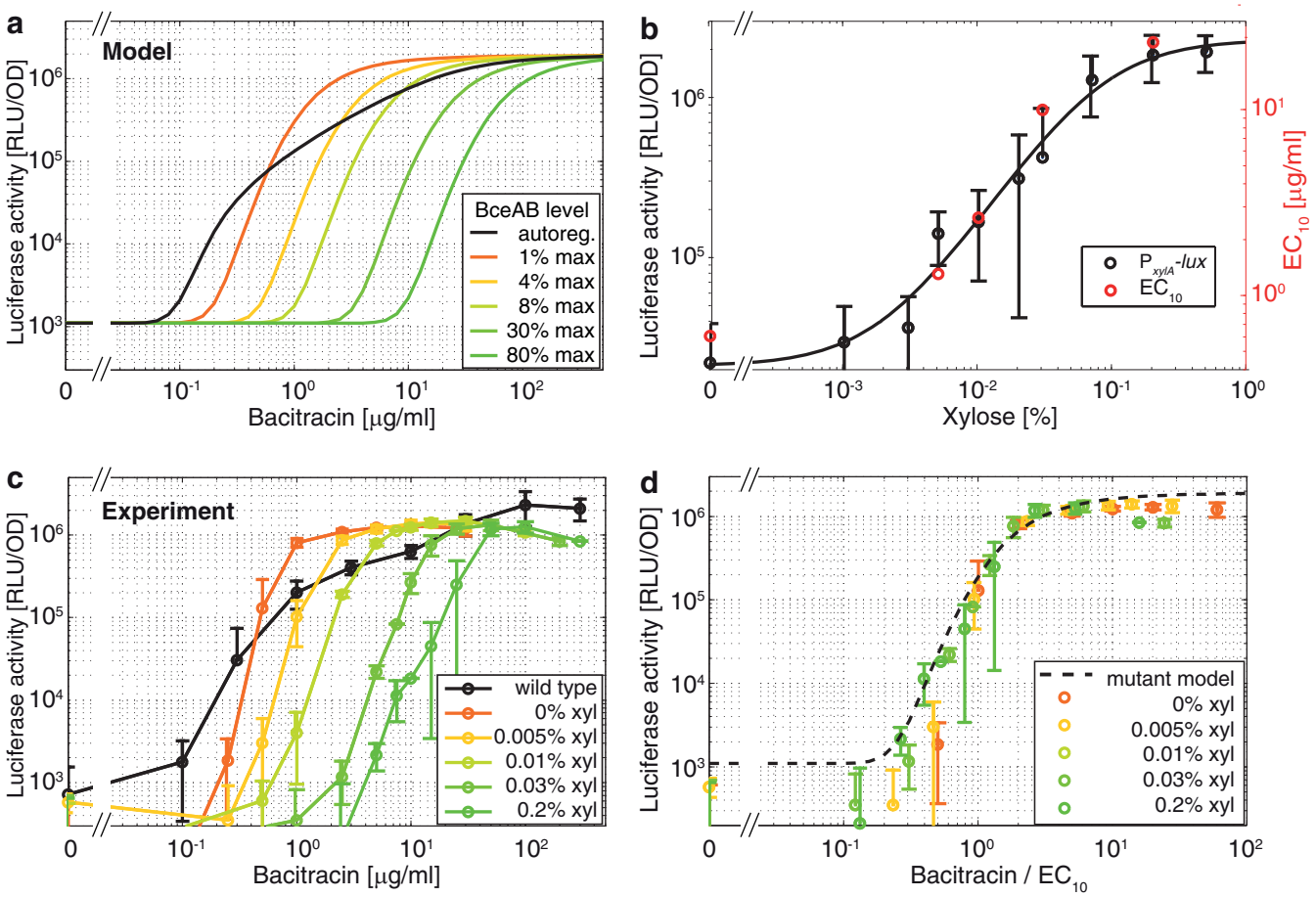

FIG 3 Signature of a relative flux sensor. (a) Theoretical prediction of P_{bceA}-*luxABCDE* dose-response curves for various levels of constitutive BceAB transporter production (colored curves), compared to the wild type with autoregulated *bceAB* expression (black curve). The expression levels of *bceAB* in the legend are percentages of the maximal P_{bceA} expression level in the wild type. These expression levels were derived from the experimental dose-response curve of the P_{xylA} promoter in panel b, which drives expression of *bceAB* in the experimental system in panel c. (b) Xylose-dependent dose-response curve of a P_{xylA}-*luxABCDE* reporter strain (black symbols) published previously (22) and fitted by a Hill function (black curve). In addition, the EC_{10} values , i.e., concentrations at which the dose-response curves in panel c reach 10% of their maximal activity, are shown as a function of xylose concentration (red symbols). (c) Experimental P_{bceA}-*luxABCDE* dose-response curves in strain SGB218, in which the endogenous chromosomal *bceAB* locus has been deleted and transporter expression is constitutively driven from a chromosomally integrated xylose-dependent P_{xylA}-*bceAB* construct (colored symbols). The wild-type dose-response curve (black symbols) was derived from strain SGB073. (d) Data from panels a and c with the *x* axis rescaled by the respective EC_{10} values. For details, see the text.

for each xylose concentration and thus also to the parameter-free predictions for the shifts in the activation threshold of P_{bceA} discussed above (Fig. 3a).

Figure 3c shows the bacitracin-dependent P_{bceA} activity of SGB218 cells grown in the presence of the selected xylose concentrations. Strikingly, we found that both the theoretically predicted abrupt onset of activation and the shift in induction threshold with increasing xylose concentration were quantitatively reflected in our experimental results. The latter becomes manifest, for instance, when EC_{10} values (the bacitracin concentration at which the dose-response reached 10% of its maximum) are plotted as a function of xylose concentration. Theoretically, the EC_{10} is expected to be proportional to the concentration of BceAB in the cell and, accordingly, to reflect the level of P_{xylA} promoter activity (Fig. 3b). Indeed, the experimental EC_{10} values all fell along this curve (Fig. 3b), suggesting (i) that P_{xylA} activity is in fact proportional to BceAB protein levels and (ii) that the number of BceAB transporters per cell determines how much bacitracin the cell will tolerate before signaling is activated. To inspect the shape of the dose-response curves in Fig. 3c more closely, we rescaled all *x* axes to the EC_{10} values. When this was done, all dose-response curves collapsed onto a single master curve (Fig. 3d). Remarkably, the experimental data points showed an even steeper increase than predicted by our model (Fig. 3d), highlighting the strong cooperativity involved in signal perception, transduction, and gene regulation at P_{bceA}. Considering that sensory perception and signaling by the Bce system involve a multiprotein complex (9), it is not difficult to envisage such strongly cooperative effects arising. Moreover, it was previously shown that many promoters of *bceAB*-like operons contain binding sites for two dimers of the response regulator (23). Indeed, P_{bceA} also possesses two BceR binding sites, spaced 13 bp apart and located directly upstream of the −10/−35 promoter elements. We recently showed that both binding sites are required for bacitracin-dependent induction of P_{bceA} (C. Fang and T. Mascher, unpublished data). Since each binding site consists of a repeat sequence, each site will likely be

occupied by a dimer of BceR, indicating that a total of four BceR molecules are required for promoter induction, which could further enhance cooperativity in signaling.

The model successfully predicts inhibitory concentrations of bacitracin. Bacitracin acts by binding to the lipid carrier UPP and preventing its dephosphorylation (19). Due to its essentiality for cell growth, a certain minimal fraction of free lipid carrier is needed to maintain cell wall biosynthesis at a given growth rate, and blocking a larger fraction of UPP is thus lethal. Intuitively, expression of the BceAB transporter is expected to release UPP from the inhibitory grip of bacitracin and thereby keep a significant fraction of UPP bacitracin free. Hence, BceAB expression should directly affect the bacitracin-bound UPP levels in the cell and, with that, the cellular sensitivity to inhibition by bacitracin.

To analyze the physiological implications of the flux-sensing mechanism, we first calculated the fraction of bacitracin-bound UPP in the cell using our mathematical model. For the wild-type strain employing bacitracin-dependent feedback regulation of *bceAB* expression, the fraction of bacitracin-bound UPP first increases rapidly with the applied concentration of the antibiotic (Fig. 4a). As soon as BceS detects a significant bacitracin flux via the BceAB transporter (at ca. 0.3 μg/ml bacitracin), transporter production is up-regulated and the rate of accumulation of bacitracin-bound UPP is slowed. Based on the bacitracin concentration needed to inhibit the growth of the wild type (ca. 200 μg/ml), we calculated the lethal fraction of bacitracin-bound UPP to be 90% (Fig. 4a). In the absence of BceAB transporters, our model predicted that the fraction of bacitracin-bound UPP increases rapidly with the applied bacitracin concentration and reaches the lethal 90% threshold at 2 μg/ml bacitracin (Fig. 4a). This is slightly below the experimentally determined MIC of 8 to 16 μg/ml for a strain with *bceAB* deleted. However, the difference is not surprising given that the model does not take into account residual bacitracin resistance caused, e.g., by the UPP phosphatase BcrC and other members of the σ^M, σ^X, and σ^W regulons involved in the response of *B. subtilis* to cell envelope stress (24–26). In contrast to the homeostatic control seen in the wild type, for the strain with constitutive *bceAB* expression, the model predicted the binding curve to be of the same shape as in the absence of BceAB. However, the curves were shifted to ever-higher bacitracin concentrations the more transporter was present in the cell (Fig. 4a). Hence, the model also predicted that the higher the level of BceAB, the greater the antibiotic concentration required for killing (Fig. 4a).

To confront these predictions with experimental data, we assayed the reporter strains for growth inhibition by bacitracin. For this, growth rates were determined after addition of a range of bacitracin concentrations to exponentially growing cultures producing different levels of transporter. For each culture, increasing the added concentration of bacitracin first led to a significant decrease in growth rate (Fig. 4b) and eventually to complete cessation of growth or cell lysis, with higher concentrations being required to inhibit cells expressing *bceAB* at higher levels. Prediction of the lethal threshold concentration by the model approximately reproduced the observed relationship between growth inhibition and *bceAB* expression (dashed line in Fig. 4b). The steeper decline of the theoretical curve compared to the experimental data at low levels of BceAB can again be explained by the presence of alternative resistance determinants in *B. subtilis*, as discussed above. When we adjusted the model to the background resistance of a *bceAB* deletion-containing strain (here, 15 μg/ml), it accurately described the correlation between BceAB expression levels and inhibitory bacitracin concentration (solid line in Fig. 4b).

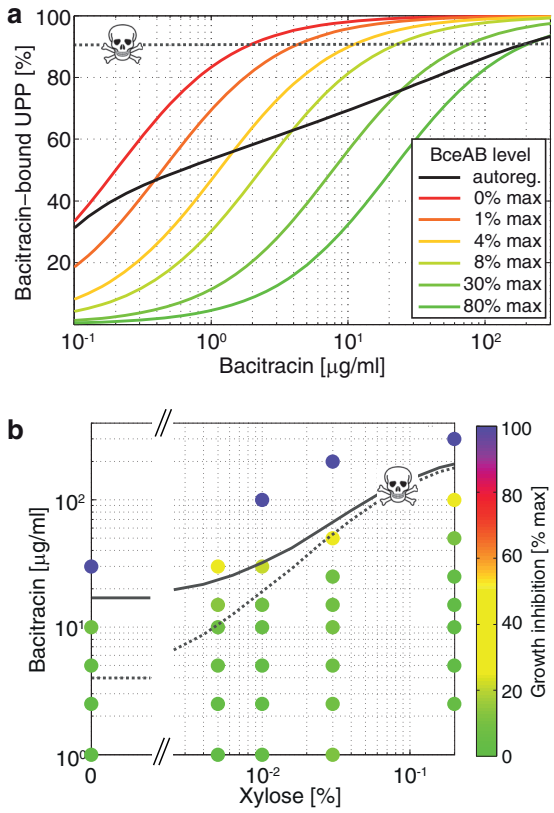

FIG 4 Inhibition of cell wall biosynthesis by blocking UPP recycling. (a) Change in the fraction of bacitracin-bound UPP as a function of external bacitracin, predicted by a model with feedback regulation (black curve) and a model with the indicated levels of constitutive *bceAB* expression (colored curves). In addition to the *bceAB* expression levels used in Fig. 3, the red curve shows the percentage of bacitracin-bound UPP in the absence of the BceAB transporter. Assuming that cell wall biosynthesis can be maintained as long as the percentage of blocked UPP carrier molecules remains below a given limit (dashed grey line), the intersection with the solid lines leads to a prediction of how the bacitracin MIC should scale with increasing BceAB expression level (dashed grey line in panel b). (b) Growth inhibition of strain SGB218 with constitutive transporter expression from a xylose-dependent P_{xylA}-*bceAB* construct (colored symbols). Cultures with a low *bceAB* expression level (0% xylose) are more susceptible to bacitracin than cultures with a high *bceAB* expression level (0.2% xylose). The model quantitatively captures the scaling of this growth inhibition line (solid grey line), when background resistance mechanisms, which are reflected in an additive offset for low *bceAB* expression level, are taken into account.

Our model does not distinguish between the cellular concentration of UPP-bacitracin complexes (i.e., the assumed transport substrate) and the true transport flux as input parameters, because binding kinetics and transport activity are mathematically equivalent in the Michaelis-Menten equation employed. This consideration becomes important in light of the possibility that BceAB might serve as a sensor without actually translocating any of its substrate. However, if BceAB were transport deficient, the concentration of UPP-associated bacitracin should always be proportional to the extracellular antibiotic concentration, regardless of the number of functional transporters in the cell. This is entirely inconsistent with the shifts in dose-response curves observed in cells expressing different amounts of BceAB (Fig. 3). Furthermore,

the good fit between observed growth inhibition by bacitracin and predicted lethal threshold at different transporter expression levels (Fig. 4) showed that the transporter indeed had an impact on the fraction of bacitracin-bound UPP and thus must be able to translocate its substrate.

Taken together, our theoretical and experimental data clearly indicate that a combination of relative flux sensing and concomitant negative feedback provides efficient homeostatic control over the level of bacitracin-bound UPP, allowing it to be maintained below the lethal concentration threshold over a range of antibiotic concentrations covering at least two orders of magnitude.

DISCUSSION

Bacteria can perceive their environment either directly, by monitoring the concentration of a relevant substance, or indirectly, by monitoring the effects on cellular physiology caused by a particular condition. We show here that sensing of transport flux of antimicrobial substances through a resistance pump presents a third and novel sensing strategy, by which the cell can directly monitor and respond to its current detoxification capacity. Through quantitative, time-resolved analysis of the dose-response dynamics, combined with mathematical modeling of the regulatory pathway, we obtained evidence that the Bce system of *B. subtilis* implements such a flux sensor, where the parameter monitored by the signaling system is the activity of individual BceAB transporters. This elegant mechanism permits continual assessment of the most critical parameter of antibiotic resistance, i.e., the cell's current capacity to deal with the inhibitory effects of the applied drug. From a systems perspective, this parameter is far more relevant to the cell than the present concentration of the antibiotic: as long as the cell's transport capacity is sufficient to detoxify the drug, there is no need for a further response even at high antibiotic concentrations. We therefore propose that flux sensing is a very cost-efficient regulatory strategy to control antibiotic resistance. To our knowledge, this is the first report of such a regulatory mechanism in any physiological context.

Over 200 Bce-like systems can currently be found in protein databases, and their components were shown to have coevolved (23). Combined with experimental confirmation of the transporter's sensory role in all systems studied to date (8, 11, 27–29), this tight evolutionary correlation suggests conservation of the signaling mechanism. Flux sensing may therefore be a widespread regulatory principle in antimicrobial peptide resistance. Because this mechanism relies on the intricate process of communicating transport flux between proteins, it should, conceivably, be easy to disrupt and thus might constitute a prime drug target to counteract resistance in pathogenic bacteria possessing Bce-like systems, such as *S. aureus*, *E. faecalis*, *Listeria monocytogenes*, and *Clostridium difficile* (8, 23, 27, 30).

Our modeling approach not only has provided evidence for a flux-sensing mechanism but also has given access to important system variables that are difficult to quantify experimentally, most notably the fraction of bacitracin-bound UPP. Analysis of such "hidden" parameters can lead to highly relevant predictions for bacterial physiology, such as our calculation of the dependence between the bacitracin concentration required to inhibit growth and the expression level of the resistance determinant. Ultimately, such an approach may have important implications for the treatment of infectious disease caused by drug-resistant bacteria. Importantly, Bce-like systems have been shown to respond to a large variety of peptide antibiotics that interfere with different stages of cell wall synthesis, including lantibiotics such as nisin, but also the clinically relevant glycopeptides vancomycin and teicoplanin (6, 31, 32).

In summary, we report the first observation of transport flux sensing as an elegant way of implementing adaptation via negative feedback regulation. We propose that this represents a highly cost-efficient mode of gene regulation, finely adjusted to the current physiological needs of the cell. In the case of antibiotic resistance mediated by Bce-like systems, this need is an increased demand for detoxification. Future exploration of further systems employing transporters to control a signaling pathway will show if this mechanism can also be found in other physiological contexts.

MATERIALS AND METHODS

Bacterial strains and growth conditions. All strains used in this study are listed in Table S3 in the supplemental material. Strains were routinely propagated in Luria-Bertani (LB) medium. For all functional assays, *B. subtilis* was grown in chemically defined CSE medium (33), in which the carbon source was modified to provide constant growth rates over an extended period of time [3.3 g/liter $(NH_4)_2SO_4$, 29 mM KH_2PO_4, 70 mM K_2HPO_4, 1× III′ salts (100× III′ salts is 0.232 g/liter $MnSO_4{\cdot}4H_2O$, 12.3 g/liter $MgSO_4{\cdot}7H_2O$), 50 mg/liter tryptophan, 22 mg/liter ammonium ferric citrate, 0.8% (wt/vol) potassium glutamate, 0.6% (wt/vol) sodium succinate, 2.5% (wt/vol) fructose]. Selective medium for *B. subtilis* contained kanamycin (10 mg/liter), chloramphenicol (5 mg/liter) or erythromycin (1 mg/liter) in combination with lincomycin (25 mg/liter) for macrolide-lincosamide-streptogramin B resistance (MLS^r). Selective medium for *E. coli* contained ampicillin (100 mg/liter). Solid medium additionally contained 1.5% (wt/vol) agar.

Construction of plasmids and strains. All cloning was performed according to BioBrick standard RFC10 (http://hdl.handle.net/1721.1/45138) or RFC25 (http://hdl.handle.net/1721.1/45140). Plasmids, strains, and primer sequences are listed in Table S3 in the supplemental material. The *bceAB* operon of *B. subtilis* was adapted to the BioBrick standard by addition of prefix and suffix sequences according to a modified RFC25 standard (22) using PCR (primers TM2577 and TM2578). All internal PstI sites were changed from CTGCAG to CTCCAG and EcoRI sites from GAATTC to GAGTTC by PCR overlap extension mutagenesis (34). Point mutations were chosen so to avoid any change in the encoded protein sequence. Cloning of the resulting fragment into the EcoRI and SpeI sites of pSB1A3 resulted in pNTSB103. The P_{xylA} region of pXT was adapted for BioBrick cloning by the addition of RFC10 prefix and suffix sequences via PCR (primers iGEM134 and iGEM135) and cloning into the EcoRI and SpeI sites of pSB1A3, to generate pNTSB104. Subsequently, the *bceAB* operon was placed under the transcriptional control of P_{xylA} by BioBrick assembly of the pNTSB103 and pNTSB104 inserts into the vector pBS2E (22), resulting in pNT2E01. To quantify target promoter activities, wild-type *B. subtilis* W168 was transformed with a transcriptional P_{bceA}-*luxABCDE* reporter construct, pSDlux101 (35), producing strain SGB073. Introduction of the same reporter together with pNT2E01 into the *bceAB*::Kan deletion strain TMB035 produced strain SGB218.

Luciferase assays. Luciferase activities were assayed using a Synergy2 multimode microplate reader from BioTek (Winooski, VT) controlled by the software Gen5. Aliquots of culture (100 μl) were added to 96-well plates (black walls, clear bottoms; Greiner Bio-One, Frickenhausen, Germany), which were incubated at 37°C with medium-intensity agitation. Cell growth was monitored by measuring optical density at 600 nm (OD_{600}). For each individual sample, the OD_{600} and relative luminescence units (RLU) (endpoint reads; 1-s integration time; sensitivity, 200) were background corrected by subtracting the respective values measured for wells containing 100 μl of CSE medium. RLU/OD_{600} values were calculated for individual measurements. Means and standard deviations

of RLU/OD_{600} values were determined from at least three biological replicates.

To synchronize cultures, 10 ml of CSE medium in a 125-ml flask was inoculated with 0.2 ml of an overnight culture and incubated at 37°C with agitation (200 rpm) to an OD_{600} of 0.2 to 0.5. Cultures were then diluted in fresh CSE medium to an OD_{600} of 0.05 and transferred to 96-well plates. OD_{600} and luminescence were monitored every 10 min, and at an OD_{600} of ~0.1 (corresponding to an OD_{600} of ~0.4 in cuvettes with a 1-cm light path length), 5 μl of Zn^{2+} bacitracin was added to give the final concentrations indicated in the figure legends. Incubation was continued, and OD_{600} and luminescence were monitored every 5 min for 1 h. For controlled expression of *bceAB* in strain SGB218, xylose was added to all growth media at the final concentrations indicated in the figure legends.

Bacitracin sensitivity assays. The MIC of bacitracin for *B. subtilis* grown in CSE medium was determined by a broth dilution technique. Cultures were grown to stationary phase in CSE medium and then diluted (1:500) into fresh CSE medium containing different concentrations of Zn^{2+} bacitracin. Following 20 to 24 h of incubation at 37°C with agitation, the MIC was scored as the lowest concentration at which no growth was observed. Inhibition of growing cultures (Fig. 4b) was determined as follows. Cells of strain SGB218 were cultured with the indicated xylose concentrations and challenged with the final concentrations of Zn^{2+} bacitracin indicated in the figure legends as described for the luciferase assays above. Average growth rates (γ) were estimated from an exponential fit to the growth curve (OD_{600}) from 0 h (bacitracin addition) to 1 h for each experimental condition. Growth inhibition was calculated as $1 - (\gamma/\gamma_{max})$, where γ_{max} is the maximal growth rate at a given xylose concentration.

Mathematical model and parameter estimation. The minimal model for the dynamics of the *bceAB* operon in the wild-type strain SGB073 is described by equations 1 to 3. In constructing this model we made the simplifying assumption that the maximal amount of UPP in a cell, UPP_{tot}, is given by the sum of all intermediate forms of the lipid carrier molecule present in the cell (see Table S1 in the supplemental material for parameter values). Binding of bacitracin to UPP then leads to the accumulation of the bacitracin-bound form of UPP, UPP-bac, to the maximal amount (UPP_{tot}). To model the constitutive expression of *bceAB* in strain SGB218, the flux-dependent transcription rate in equation 2 was replaced by a temporally constant transcription rate, which is determined solely by the concentration of externally supplied xylose:

$$\frac{d}{dt}[m] = \alpha_{xyl} - \lambda[m] \tag{4}$$

The xylose-dependent rate of *bceAB* transcription driven by P_{xylA} was modeled as $\alpha_{xyl} = \alpha \times f(xyl)/g(\mathrm{bac}=0)$, where α is the rate of P_{bceA}-controlled transcription in the absence of bacitracin and $f(xyl)$ and $g(\mathrm{bac})$ are the experimental dose-response curves for P_{xylA} (Fig. 3b) and P_{bceA} (Fig. 2B), respectively. In addition, expression of the *luxABCDE* reporter genes in all strains is under the control of an ectopically integrated P_{bceA} promoter, which is assumed to follow the same transcriptional kinetics as the promoter at its native genomic locus (cf. equation 2):

$$\frac{d}{dt}[m_{lux}] = \alpha\frac{1 + \omega\left(J_{\mathrm{bac}}/\kappa\right)^n}{1 + \left(J_{\mathrm{bac}}/\kappa\right)^n} - \lambda_{lux}[m_{lux}] \tag{5}$$

Here, m_{lux} is the *luxABCDE* mRNA, λ_{lux} is the associated degradation rate, and all other parameters are the same as in equation 2. Assuming that one of the proteins in the *lux* operon is rate limiting for light production, its dynamics is modeled by

$$\frac{d}{dt}[\mathrm{Lux}] = \beta[m_{lux}] - \delta_{lux}[\mathrm{Lux}] \tag{6}$$

where β is the translation rate and δ_{lux} is the corresponding protein half-life. In addition, a multiplicative scaling factor, σ, was introduced to relate the Lux protein level to the experimentally measured luminescence output.

To fit the model to our experimental data, the parameters were fixed to physiological values whenever possible (see Table S1 in the supplemental material) and constrained to physiologically reasonable intervals in all other cases (see Table S2 in the supplemental material). Then, a trust region-reflective Newton method (MatLab; The MathWorks, Inc.) was used to minimize the value of χ^2 between the dose-response curve in Fig. 2B and the model. To account for the presence of local optima and to quantify the uncertainty in the estimated parameters, 100 independent fits were performed with randomly chosen initial parameter sets (see Fig. S4 and S5 in the supplemental material for correlation graphs between χ^2 and estimated parameters). Confidence intervals for the fitted parameters (see Table S2) were obtained as previously described (36). The prediction of the dose-response curves for strain SGB218 was based on the parameter set from strain SGB073, but calculated using equation 4 instead of equation 2.

SUPPLEMENTAL MATERIAL

Supplemental material for this article may be found at http://mbio.asm.org/lookup/suppl/doi:10.1128/mBio.00975-15/-/DCSupplemental.

Figure S1, EPS file, 0.5 MB.
Figure S2, EPS file, 0.1 MB.
Figure S3, TIF file, 2.3 MB.
Figure S4, EPS file, 0.8 MB.
Figure S5, EPS file, 2 MB.
Table S1, DOCX file, 0.1 MB.
Table S2, DOCX file, 0.1 MB.
Table S3, DOCX file, 0.02 MB.

ACKNOWLEDGMENTS

Work in the labs of U.G., T.M., and G.F. was funded through the Deutsche Forschungsgemeinschaft (DFG) in the context of the Priority Program SPP 1617 "Phenotypic Heterogeneity and Sociobiology of Bacterial Populations" (GE1098/6-1 to U.G., MA2837/3-1 to T.M., and a start-up grant to G.F.). Work in S.G.'s lab was funded by a DFG research grant (GE2164/3-1).

We thank Ina Lackerbauer for technical assistance in strain construction and Ulrike Mäder for determination of the *bceAB* mRNA half-life. We are also grateful to Laurence Hurst for valuable suggestions during the writing process and to Jim Caunt for critical reading of the manuscript.

G.F. performed all mathematical modeling; S.D., N.S.T., and J.R. performed the experiments; S.G. coordinated experimental work; T.M., U.G., G.F., and S.G. designed the study; G.F. and S.G. wrote the manuscript; all authors approved the manuscript.

REFERENCES

1. **Kwun MJ, Hong H-J.** 2014. The activity of glycopeptide antibiotics against resistant bacteria correlates with their ability to induce the resistance system. Antimicrob Agents Chemother **58:**6306–6310. http://dx.doi.org/10.1128/AAC.03668-14.
2. **Andersson DI, Hughes D.** 2010. Antibiotic resistance and its cost: is it possible to reverse resistance? Nat Rev Microbiol **8:**260–271. http://dx.doi.org/10.1038/nrmicro2319.
3. **Koteva K, Hong HJ, Wang XD, Nazi I, Hughes D, Naldrett MJ, Buttner MJ.** 2010. A vancomycin photoprobe identifies the histidine kinase VanSsc as a vancomycin receptor. Nat Chem Biol **6:**327–329.
4. **Wolf D, Domínguez-Cuevas P, Daniel RA, Mascher T.** 2012. Cell envelope stress response in cell wall-deficient L-forms of *Bacillus subtilis*. Antimicrob Agents Chemother **56:**5907–5915. http://dx.doi.org/10.1128/AAC.00770-12.
5. **Rietkötter E, Hoyer D, Mascher T.** 2008. Bacitracin sensing in *Bacillus subtilis*. Mol Microbiol **68:**768–785. http://dx.doi.org/10.1111/j.1365-2958.2008.06194.x.
6. **Gebhard S, Mascher T.** 2011. Antimicrobial peptide sensing and detoxification modules: unravelling the regulatory circuitry of *Staphylococcus aureus*. Mol Microbiol **81:**581–587. http://dx.doi.org/10.1111/j.1365-2958.2011.07747.x.
7. **Gebhard S.** 2012. ABC transporters of antimicrobial peptides in Firmic-

utes bacteria—phylogeny, function and regulation. Mol Microbiol **86:** 1295–1317. http://dx.doi.org/10.1111/mmi.12078.
8. **Hiron A, Falord M, Valle J, Débarbouillé M, Msadek T.** 2011. Bacitracin and nisin resistance in *Staphylococcus aureus*: a novel pathway involving the BraS/BraR two-component system (SA2417/SA2418) and both the BraD/BraE and VraD/VraE ABC transporters. Mol Microbiol **81:** 602–622. http://dx.doi.org/10.1111/j.1365-2958.2011.07735.x.
9. **Dintner S, Heermann R, Fang C, Jung K, Gebhard S.** 2014. A sensory complex consisting of an ATP-binding cassette transporter and a two-component regulatory system controls bacitracin resistance in *Bacillus subtilis*. J Biol Chem **289:**27899–27910. http://dx.doi.org/10.1074/jbc.M114.596221.
10. **Mascher T.** 2014. Bacterial (intramembrane-sensing) histidine kinases: signal transfer rather than stimulus perception. Trends Microbiol **22:** 559–565. http://dx.doi.org/10.1016/j.tim.2014.05.006.
11. **Staroń A, Finkeisen DE, Mascher T.** 2011. Peptide antibiotic sensing and detoxification modules of *Bacillus subtilis*. Antimicrob Agents Chemother **55:**515–525. http://dx.doi.org/10.1128/AAC.00352-10.
12. **Hasty J, McMillen D, Isaacs F, Collins JJ.** 2001. Computational studies of gene regulatory networks: *in numero* molecular biology. Nat Rev Genet **2:**268–279. http://dx.doi.org/10.1038/35066056.
13. **Rosenfeld N, Elowitz MB, Alon U.** 2002. Negative autoregulation speeds the response times of transcription networks. J Mol Biol **323:**785–793. http://dx.doi.org/10.1016/S0022-2836(02)00994-4.
14. **Island MD, Kadner RJ.** 1993. Interplay between the membrane-associated UhpB and UhpC regulatory proteins. J Bacteriol **175:** 5028–5034.
15. **Schwöppe C, Winkler HH, Neuhaus HE.** 2003. Connection of transport and sensing by UhpC, the sensor for external glucose-6-phosphate in *Escherichia coli*. Eur J Biochem **270:**1450–1457. http://dx.doi.org/10.1046/j.1432-1033.2003.03507.x.
16. **Schleif R.** 2000. Regulation of the L-arabinose operon of *Escherichia coli*. Trends Genet **16:**559–565. http://dx.doi.org/10.1016/S0168-9525(00)02153-3.
17. **Chang G.** 2003. Multidrug resistance ABC transporters. FEBS Lett **555:** 102–105. http://dx.doi.org/10.1016/S0014-5793(03)01085-8.
18. **Ohki R, Giyanto, Tateno K, Masuyama W, Moriya S, Kobayashi K, Ogasawara N.** 2003. The BceRS two-component regulatory system induces expression of the bacitracin transporter, BceAB, in *Bacillus subtilis*. Mol Microbiol **49:**1135–1144. http://dx.doi.org/10.1046/j.1365-2958.2003.03653.x.
19. **Storm DR, Strominger JL.** 1973. Complex formation between bacitracin peptides and isoprenyl pyrophosphates. The specificity of lipid-peptide interactions. J Biol Chem **248:**3940–3945.
20. **Bintu L, Buchler NE, Garcia HG, Gerland U, Hwa T, Kondev J, Phillips R.** 2005. Transcriptional regulation by the numbers: models. Curr Opin Genet Dev **15:**116–124. http://dx.doi.org/10.1016/j.gde.2005.02.007.
21. **Steinmetz PA, Wörner S, Unden G.** 2014. Differentiation of DctA and DcuS function in the DctA/DcuS sensor complex of *Escherichia coli*: function of DctA as an activity switch and of DcuS as the C4-dicarboxylate sensor. Mol Microbiol **94:**218–229. http://dx.doi.org/10.1111/mmi.12759.
22. **Radeck J, Kraft K, Bartels J, Cikovic T, Dürr F, Emenegger J, Kelterborn S, Sauer C, Fritz G, Gebhard S, Mascher T.** 2013. The *Bacillus* BioBrick box: generation and evaluation of essential genetic building blocks for standardized work with *Bacillus subtilis*. J Biol Eng **7:**29. http://dx.doi.org/10.1186/1754-1611-7-29.
23. **Dintner S, Staroń A, Berchtold E, Petri T, Mascher T, Gebhard S.** 2011. Coevolution of ABC transporters and two-component regulatory systems as resistance modules against antimicrobial peptides in Firmicutes bacteria. J Bacteriol **193:**3851–3862. http://dx.doi.org/10.1128/JB.05175-11.
24. **Cao M, Helmann JD.** 2002. Regulation of the *Bacillus subtilis bcrC* bacitracin resistance gene by two extracytoplasmic function σ factors. J Bacteriol **184:**6123–6129. http://dx.doi.org/10.1128/JB.184.22.6123-6129.2002.
25. **Cao M, Helmann JD.** 2004. The *Bacillus subtilis* extracytoplasmic-function σ^X factor regulates modification of the cell envelope and resistance to cationic antimicrobial peptides. J Bacteriol **186:**1136–1146. http://dx.doi.org/10.1128/JB.186.4.1136-1146.2004.
26. **Eiamphungporn W, Helmann JD.** 2008. The *Bacillus subtilis* σ^M regulon and its contribution to cell envelope stress responses. Mol Microbiol **67:** 830–848. http://dx.doi.org/10.1111/j.1365-2958.2007.06090.x.
27. **Gebhard S, Fang C, Shaaly A, Leslie DJ, Weimar MR, Kalamorz F, Carne A, Cook GM.** 2014. Identification and characterization of a bacitracin resistance network in *Enterococcus faecalis*. Antimicrob Agents Chemother **58:**1425–1433. http://dx.doi.org/10.1128/AAC.02111-13.
28. **Revilla-Guarinos A, Gebhard S, Alcántara C, Staron A, Mascher T, Zúñiga M.** 2013. Characterization of a regulatory network of peptide antibiotic detoxification modules in *Lactobacillus casei* BL23. Appl Environ Microbiol **79:**3160–3170. http://dx.doi.org/10.1128/AEM.00178-13.
29. **Ouyang J, Tian X-L, Versey J, Wishart A, Li Y-H.** 2010. The BceABRS four-component system regulates the bacitracin-induced cell envelope stress response in *Streptococcus mutans*. Antimicrob Agents Chemother **54:**3895–3906. http://dx.doi.org/10.1128/AAC.01802-09.
30. **Collins B, Curtis N, Cotter PD, Hill C, Ross RP.** 2010. The ABC transporter AnrAB contributes to the innate resistance of *Listeria monocytogenes* to nisin, bacitracin, and various beta-lactam antibiotics. Antimicrob Agents Chemother **54:**4416–4423. http://dx.doi.org/10.1128/AAC.00503-10.
31. **Meehl M, Herbert S, Götz F, Cheung A.** 2007. Interaction of the GraRS two-component system with the VraFG ABC transporter to support vancomycin-intermediate resistance in *Staphylococcus aureus*. Antimicrob Agents Chemother **51:**2679–2689. http://dx.doi.org/10.1128/AAC.00209-07.
32. **Pietiäinen M, François P, Hyyryläinen H-L, Tangomo M, Sass V, Sahl H-G, Schrenzel J, Kontinen VP.** 2009. Transcriptome analysis of the responses of *Staphylococcus aureus* to antimicrobial peptides and characterization of the roles of *vraDE* and *vraSR* in antimicrobial resistance. BMC Genomics **10:**429. http://dx.doi.org/10.1186/1471-2164-10-429.
33. **Stülke J, Hanschke R, Hecker M.** 1993. Temporal activation of beta-glucanase synthesis in *Bacillus subtilis* is mediated by the GTP pool. J Gen Microbiol **139:**2041–2045. http://dx.doi.org/10.1099/00221287-139-9-2041.
34. **Ho SN, Hunt HD, Horton RM, Pullen JK, Pease LR.** 1989. Site-directed mutagenesis by overlap extension using the polymerase chain reaction. Gene **77:**51–59. http://dx.doi.org/10.1016/0378-1119(89)90358-2.
35. **Kallenberg F, Dintner S, Schmitz R, Gebhard S.** 2013. Identification of regions important for resistance and signalling within the antimicrobial peptide transporter BceAB of *Bacillus subtilis*. J Bacteriol **195:**3287–3297. http://dx.doi.org/10.1128/JB.00419-13.
36. **Wall ME, Markowitz DA, Rosner JL, Martin RG.** 2009. Model of transcriptional activation by MarA in *Escherichia coli*. PLoS Comput Biol **5:**e1000614. http://dx.doi.org/10.1371/journal.pcbi.1000614.